

# Negative refraction and the minimum lattice cell size

Igor Tsukerman

Department of Electrical and Computer Engineering, The University of Akron, Akron, Ohio 44325-3904, USA  
(E-mail: igor@uakron.edu)

Received January 3, 2008; revised March 14, 2008; accepted March 15, 2008;  
posted April 2, 2008 (Doc. ID 91224); published May 15, 2008

Artificial periodic structures (metamaterials and photonic crystals) with feature sizes smaller than the wavelength can be capable of supporting backward waves and producing negative refraction. However, backward waves may only exist if the lattice cell size is a sufficiently large fraction of the vacuum wavelength and/or the Bloch wavelength. Explicit lower bounds for the cell size are established and imply, in particular, a limit on the optical resolution of negative-index lenses. A key tool in the analysis is Fourier decomposition of Bloch waves and related eigenfrequency estimates. Numerical examples and a detailed exposition of the mechanism of backward waves are included. © 2008 Optical Society of America  
OCIS codes: 350.4238, 160.3820, 260.2110, 100.6640, 050.5298.

## 1. INTRODUCTION

Negative refraction (electromagnetic waves bending the “wrong” way at material interfaces) and the closely related phenomenon of backward waves (phase velocity at an obtuse angle with group velocity) have become one of the most fascinating areas of research in nanophotonics this century with hundreds of published research papers and a number of books and review papers readily available, Pendry and Smith [1], Milonni [2], Eleftheriades and Balmain [3], Ramakrishna [4], and others.

As early as the 1940s, Mandelshtam pointed out [5,6] that waves would negatively refract at the interface boundary between a regular and a backward-wave medium. In 1967, Veselago [7] showed that media with simultaneously negative dielectric permittivity  $\epsilon$  and magnetic permeability  $\mu$  would support backward waves and exhibit other unusual behavior of wave propagation and refraction. (The English translation [7] of Veselago’s paper appeared in 1968.)

A turning point in the research on double-negative materials came in 1999–2000, when Pendry *et al.* [8] theoretically showed and Smith *et al.* [9] experimentally confirmed negative refraction in an artificial material with split-ring resonators (SRRs). Furthermore, Pendry discovered that Veselago’s unusual “lens” (a slab of a negatively refracting material) could produce a perfect image of a point source, thereby beating the diffraction limit [10]. While Veselago’s description of his lens purely relied on geometric optics, Pendry’s electromagnetic analysis showed that the evanescent part of light emitted by the source is “amplified” by the slab, with the ultimate result of perfect transmission and focusing of both propagating and evanescent components of the wave. The first, to the best of my knowledge, publication on what today would be called a (quasi)-perfect cylindrical lens was in 1994 Nicorovici *et al.* [11]. Now more detailed follow-up papers by Milton and Nicorovici [12] and Milton *et al.* [13] are available.

Truly homogeneous materials, in the Veselago sense, are not currently known. Consequently, much effort has been devoted to the development of artificial metamaterials capable of supporting backward waves and producing negative refraction. Selected developments are as follows (all frequencies approximate): Smith *et al.* [9] (copper SRR and wires, 4.85 GHz, 2000); Shelby *et al.* [14] (copper SRR and strips, 10 GHz, 2001); Parazzoli *et al.* [15] (a stack of SRRs with metal strips, 12.6 GHz, 2003); Houck *et al.* [16] (composite wire and SRR prisms, 10 GHz, 2003); Smith and Vier [17] (copper SRR and strips, 11 GHz, 2004); Shalaev [18] (pairs of nanorods, 200 THz, 2005–2007); Zhang *et al.* [19] (nanofishnet with elliptical voids, 170 THz, 2006); Dolling *et al.* [20,21] (nanofishnet with rectangular voids, 210 THz, 380 THz, 2006–2007).

Separately from the progress in metamaterials, negative refraction was observed and analyzed in singly and doubly periodic waveguides (Zengerle [22], late 1970s–1980s) and in photonic crystals (Notomi [23] in 2000). Since 2000, there have been a number of publications on negative refraction and the associated lensing effects in photonic crystals: Luo *et al.* [24], “all-angle negative refraction” in a bcc lattice of air cubes in a dielectric; Cubukcu *et al.* [25], experimental and theoretical demonstration of negative refraction and superlensing in a 2D photonic crystal in the microwave range; Moussa *et al.* [26], experimental and theoretical study of negative refraction and superlensing in a triangular array of rectangular dielectric bars; Yannopapas and Moroz [27] and Wheeler *et al.* [28], negative refraction in a lattice of polaritonic spheres. See also Parimi *et al.* [29] (left-handed behavior of the waves in a triangular lattice of cylindrical copper rods). An example due to Gajic *et al.* [30] and Meisels *et al.* [31] is discussed later in this paper.

In the designs cited above, the cell size as a fraction of the vacuum wavelength varies between  $\sim 0.11/0.42$ . One might hope that further improvements in nanofabrication and design could bring the cell size down to a smaller

fraction of the wavelength, thereby approaching the Veselago case of a homogeneous material. However, the main message of this paper is that the cell size is constrained not only by fabrication technologies but by fundamental lower bounds as well.

The objective of this paper is twofold: (i) to clarify the mechanism of negative refraction and backward waves in periodic structures and (ii) to show that backward waves disappear in the homogenization limit and to establish a lower bound for the lattice cell size of materials capable of supporting backward waves.

The remainder of this paper is organized as follows. First, following Veselago, Section 2 reviews wave propagation in a (hypothetical) medium with simultaneously negative  $\epsilon$  and  $\mu$ . Sections 3, 4, and 6 provide background information on the governing equations in real and Fourier space. Section 5 stresses the dependence of refractive behavior on both intrinsic and extrinsic characteristics of the Bloch wave (i.e., on its forward/backward character in the bulk as well as on the “excitation channel” at the interface). Finally, Section 7 establishes the main result of this paper, lower bounds for the lattice cell size of negative-index periodic media. Numerical examples are given and the implications for the optical resolution are noted.

## 2. FORWARD AND BACKWARD PLANE WAVES IN A HOMOGENEOUS ISOTROPIC MEDIUM

This section examines backward waves in a hypothetical homogeneous isotropic medium with unusual material parameters (the “Veselago medium”). Subsequently, we shall turn to the analysis of forward and backward Bloch waves in periodic dielectric structures. Even though the final result of this section is now well established, the derivation below may be instructive as it does not rely on any supplementary considerations, such as analyticity of the index of refraction, the sign of its imaginary part, or causality (see Milonni [2], Pokrovsky and Efros [32], and Ziolkowski and Heyman [33] for discussions of these matters and McCall *et al.* [34] for a similar analysis).

Consider the behavior of plane waves in a homogeneous isotropic medium with arbitrary constant complex parameters  $\epsilon$  and  $\mu$  at a given frequency. The only stipulation is that the medium be passive (no generation of energy), which under the  $\exp(-i\omega t)$  phasor convention implies positive imaginary parts  $\epsilon''$  and  $\mu''$  of  $\epsilon$  and  $\mu$ . It will be helpful to assume that these imaginary parts are *strictly positive* and to view lossless materials as a limiting case of small losses,  $\epsilon'' \rightarrow +0$ ,  $\mu'' \rightarrow +0$ . The goal is to establish conditions for the plane wave to be forward or backward. In the latter case, one has a Veselago medium.

Let the plane wave propagate along the  $x$  axis, with  $E = E_y$  and  $H = H_z$

$$E = E_y = E_0 \exp(ikx), \quad (1)$$

$$H = H_z = H_0 \exp(ikx), \quad (2)$$

where  $E_0$  and  $H_0$  are some complex amplitudes. It immediately follows from Maxwell's equations that

$$H_0 = \frac{k}{\omega\mu} E_0, \quad (3)$$

$$k = \omega\sqrt{\mu\epsilon} \quad (\text{which branch of the square root?}). \quad (4)$$

Which branch of the square root should be implied in the formula for the wavenumber? In an unbounded medium, there is complete symmetry between the  $+x$  and  $-x$  directions and waves corresponding to both branches of the root are equally valid. It is clear, however, that each of the waves is unbounded in one of the directions, which is not physical.

For a more physical picture, it is tacitly assumed that the unbounded growth is truncated, e.g., the medium and the wave occupy only half of the space, where the wave decays. With this in mind, let us focus on one of the two waves, the one with a positive imaginary part of  $k$

$$k'' > 0. \quad (5)$$

Note that Eq. (5) is not a “fundamental law” of physics [32] but just one of the two possible subcases. The other wave, with  $k'' < 0$ , is equally valid but “lives” in the other half-space; the analysis for it is completely analogous.

Splitting up the real and imaginary exponentials

$$\exp(ikx) = \exp(i(k' + ik'')x) = \exp(-k''x)\exp(ik'x)$$

we observe that the wave of Eq. (5) decays in the  $+x$  direction. On physical grounds, one can argue that the energy in this wave must flow in the  $+x$  direction as well. This can be verified by computing the time-averaged Poynting vector

$$P = P_x = \frac{1}{2} \operatorname{Re} E_0 H_0^* = \frac{1}{2} \operatorname{Re} \frac{k}{\omega\mu} |E_0|^2. \quad (6)$$

To examine the sign of  $P$ , let us express  $P$  via material parameters

$$\epsilon = |\epsilon| \exp(i\phi_\epsilon); \quad \mu = |\mu| \exp(i\phi_\mu); \quad 0 < \phi_\epsilon, \phi_\mu < \pi.$$

Then the square root with a positive imaginary part, consistent with the wave of Eq. (5) under consideration gives

$$k = \omega\sqrt{|\mu||\epsilon|} \exp\left(i \frac{\phi_\epsilon + \phi_\mu}{2}\right). \quad (7)$$

Ignoring all positive real factors irrelevant to the sign of  $P$  in Eq. (6) we get

$$\operatorname{sign} P = \operatorname{sign} \operatorname{Re} \frac{k}{\mu} = \operatorname{sign} \cos \frac{\phi_\epsilon - \phi_\mu}{2}.$$

The cosine, however, is always positive as  $0 < \phi_\epsilon, \phi_\mu < \pi$ . Thus, as expected,  $P_x$  is positive, indicating that indeed energy flows in the  $+x$  direction.

The type of the wave (forward versus backward) therefore depends on the sign of the phase velocity  $\omega/k'$ , that is, on the sign of  $k'$ . As follows from Eq. (7),

$$\text{sign } k' = \text{sign } \cos \frac{\phi_\epsilon + \phi_\mu}{2}$$

and the wave is backward if and only if the cosine is negative or

$$\phi_\epsilon + \phi_\mu > \pi. \quad (8)$$

An algebraically equivalent criterion can be derived by noting that the cosine function is monotonically decreasing on  $[0, \pi]$  and hence  $\phi_\epsilon > \pi - \phi_\mu$  is equivalent to

$$\cos \phi_\epsilon < \cos(\pi - \phi_\mu),$$

or

$$\cos \phi_\epsilon + \cos \phi_\mu < 0.$$

This coincides with the Depine–Lakhtakia condition [35] for backward waves

$$\frac{\epsilon'}{|\epsilon|} + \frac{\mu'}{|\mu|} < 0. \quad (9)$$

Expression (9) is invariant with respect to the complex conjugation and is therefore valid for both phasor conventions  $\exp(\pm i\omega t)$ .

Note that the analysis above relies only on Maxwell's equations and the definitions of the Poynting vector and phase velocity. No considerations of causality, so common in literature on negative refraction, were needed to establish the backward-wave conditions of Eqs. (8) and (9).

### 3. FIELD EQUATIONS AND BLOCH WAVES

We shall consider the usual 1D, 2D, and 3D renditions of time-harmonic Maxwell's equations. At optical frequencies, the intrinsic permeability of all media can be set to  $\mu_0$  (Landau and Lifshitz [36]). As a side note, artificial magnetism can be created in periodic dielectric structures at optical frequencies (Cai *et al.* [37] and Linden *et al.* [38]). The equivalent “mesoscopic” permeability may then be different from  $\mu_0$ , but the intrinsic microscopic permeability of the materials involved is still  $\mu_0$ .

In 1D, the equation for the  $E$ -field is

$$E''(x) + k^2 E(x) = 0, \quad (10)$$

with

$$k^2 = \omega^2 \mu_0 \epsilon(x).$$

In periodic structures with  $\epsilon$  as a periodic function of  $x$ , a fundamental solution of Eq. (10) is the Bloch–Floquet wave of the form

$$E(x) = E_{\text{PER}}(x) \exp(iK_B x), \quad (11)$$

where  $K_B$  is the Bloch wavenumber and subscript “PER” marks functions periodic over the lattice with a given cell size  $a$ .

In 2D, the  $E$ -mode (or  $s$ -mode, one-component field  $E = E_z$ ) is described by the equation

$$\nabla^2 E + k^2 E = 0,$$

with

$$k^2 = \omega^2 \mu_0 \epsilon(x, y). \quad (12)$$

Again, if  $\epsilon$  is a periodic function of coordinates, the fundamental solutions of the field equation are known to be Bloch waves with a (yet undetermined) wave vector  $\mathbf{K}_B = (K_{Bx}, K_{By})$

$$E(\mathbf{r}) = E_{\text{PER}}(\mathbf{r}) \exp(i\mathbf{K}_B \cdot \mathbf{r}); \quad \mathbf{r} \equiv (x, y). \quad (13)$$

Assuming for simplicity a square lattice cell of size  $a$ , subscript PER implies periodicity with respect to any lattice vector  $(n_x a, n_y a)$  with integer  $n_x, n_y$ .

The governing equation for the  $H$ -mode (or  $p$ -mode, one-component  $H$ -field) is

$$\nabla \cdot \epsilon^{-1} \nabla H + \omega^2 \mu_0 H = 0, \quad (14)$$

and the expression for the Bloch  $H$ -wave is completely analogous to Eq. (13).

Finally, the 3D  $\mathbf{E}$ -field equation and the corresponding Bloch wave can be written as

$$\nabla \times \nabla \times \mathbf{E} - \omega^2 \mu_0 \epsilon \mathbf{E} = 0, \quad (15)$$

$$\mathbf{E}(\mathbf{r}) = \mathbf{E}_{\text{PER}}(\mathbf{r}) \exp(i\mathbf{K} \cdot \mathbf{r}),$$

$$\mathbf{r} \equiv (x, y, z), \quad \mathbf{K}_B = (K_{Bx}, K_{By}, K_{Bz}). \quad (16)$$

The  $\mathbf{H}$ -field satisfies the wave equation

$$\nabla \times \epsilon^{-1} \nabla \times \mathbf{H} - \omega^2 \mu_0 \mathbf{H} = 0. \quad (17)$$

### 4. FOURIER HARMONICS OF BLOCH WAVES

In 1D, the periodic factor  $E_{\text{PER}}(x)$  from Eq. (11) can be expanded into a Fourier series with coefficients  $e_m$  ( $m = 0, \pm 1, \pm 2, \dots$ )

$$E_{\text{PER}}(x) = \sum_{m=-\infty}^{\infty} e_m \exp(im\kappa_0 x), \quad \kappa_0 = 2\pi a^{-1}. \quad (18)$$

The Fourier coefficients  $e_m$  are given by the usual integral expressions

$$e_m = a^{-1} \int_a E_{\text{PER}}(x) \exp(-im\kappa_0 x) dx, \quad (19)$$

where the integration is over any period of length  $a$ .

In 3D, the Bloch wave is analogous to its 2D form of Eq. (13)

$$\mathbf{E}(\mathbf{r}) = \mathbf{E}_{\text{PER}}(\mathbf{r}) \exp(i\mathbf{K}_B \cdot \mathbf{r}), \quad \mathbf{r} \equiv (x, y, z), \quad (20)$$

and the periodic factor can again be expanded into its Fourier series

$$\mathbf{E}_{\text{PER}}(\mathbf{r}) = \sum_{\mathbf{m} \in \mathbb{Z}^3} \mathbf{e}_{\mathbf{m}} \exp(i\mathbf{k}_{\mathbf{m}} \cdot \mathbf{r}), \quad (21)$$

where  $\mathbf{k}_{\mathbf{m}} = \kappa_0 \mathbf{m} \equiv \kappa_0 (m_x, m_y, m_z)$  with integers  $m_x, m_y, m_z$ , and Fourier coefficients  $\mathbf{e}_{\mathbf{m}}$ . The field is treated as vectorial for generality, even if it happens to have only one Cartesian component. Thus the Fourier expansion of the 3D Bloch wave is

$$\mathbf{E}(\mathbf{r}) = \sum_{\mathbf{m} \in \mathbb{Z}^3} \mathbf{E}_{\mathbf{m}} \equiv \sum_{\mathbf{m} \in \mathbb{Z}^3} \mathbf{e}_{\mathbf{m}} \exp(i\mathbf{k}_{\mathbf{m}} \cdot \mathbf{r}) \exp(i\mathbf{K}_B \cdot \mathbf{r}). \quad (22)$$

This representation of the Bloch wave as a suite of plane waves  $\mathbf{E}_{\mathbf{m}}$  is helpful for the analysis and physical interpretation of energy flow, phase velocity, and other properties of this wave [39].

For  $\mu = \mu_0$ , the expression for  $\mathbf{E}(\mathbf{r})$  leads, via the Maxwell  $\nabla \times \mathbf{E}$  equation, to a similar decomposition of the magnetic field

$$\mathbf{H}(\mathbf{r}) = \sum_{\mathbf{m} \in \mathbb{Z}^3} \mathbf{H}_{\mathbf{m}} \equiv \sum_{\mathbf{m} \in \mathbb{Z}^3} \mathbf{h}_{\mathbf{m}} \exp(i\mathbf{k}_{\mathbf{m}} \cdot \mathbf{r}) \exp(i\mathbf{K}_B \cdot \mathbf{r}) \quad (23)$$

with  $\mathbf{h}_{\mathbf{m}} = (\omega\mu_0)^{-1} \mathbf{k}_{\mathbf{m}} \times \mathbf{e}_{\mathbf{m}}$ . It is important to note from the outset, as Lombardet *et al.* do [39], that the individual plane-wave components of the Bloch wave do not satisfy Maxwell's equations in the periodic medium and therefore do not represent physical fields. Only taken together do these Fourier harmonics form a valid field.

It is straightforward to verify that the plane waves in the decomposition are orthogonal functions (in the mathematical sense of standard vector  $\mathbf{L}_2$  inner product) over the lattice cell. Hence, by Parseval's theorem, the time- and cell-averaged Poynting vectors  $\langle \mathbf{P} \rangle = \langle \text{Re}\{\mathbf{E} \times \mathbf{H}^*\} \rangle / 2$  can be represented as a sum of the Poynting vectors for the individual plane waves [39]

$$\langle \mathbf{P} \rangle = \sum_{\mathbf{m} \in \mathbb{Z}^3} \mathbf{P}_{\mathbf{m}}; \quad \mathbf{P}_{\mathbf{m}} = \frac{\mathbf{k}_{\mathbf{m}}}{2\omega\mu_0} |\mathbf{e}_{\mathbf{m}}|^2. \quad (24)$$

Next, group velocity  $\partial\omega/\partial\mathbf{k}$  is clearly the same for all plane-wave components and hence group velocity for the whole Bloch wave can be defined as  $\mathbf{v}_g = \partial\omega/\partial\mathbf{K}_B$ . In cases of weak dispersion, it can be shown [40,41] that this velocity, indeed, approximately represents signal velocity in the periodic medium.

## 5. INTRINSIC AND EXTRINSIC PROPERTIES

For the analysis of anomalous wave propagation and refraction, it is important to distinguish intrinsic and extrinsic characteristics of the wave. Intrinsic properties of the wave refer to its characterization as either forward or backward, that is, whether the angle between the Poynting vector and phase velocity (if the latter can be properly defined) is acute or obtuse. Extrinsic properties refer to conditions at the interface of the periodic structure with air or another homogeneous medium. A key point is that refraction at the interface depends not only on the intrinsic characteristics of the wave in the bulk but also on the way the Bloch wave is excited [39].

Indeed, any plane-wave component of the Bloch wave can serve as an excitation channel (a lucid term due to Lombardet *et al.* [39]) for this wave, provided that—for a certain angle of incidence—it matches the  $x$  component of the incident wave in the air

$$K_{Bx} + \kappa_0 m = k_x^{\text{air}}.$$

This will correspond to a propagating, rather than evanescent, wave in the air if  $|K_{Bx} + \kappa_0 m| < k^{\text{air}}$ .

Refraction properties at the interface are a function of the intrinsic characteristics of the wave in the bulk as well as the excitation channel with four substantially different possible combinations. For further details see [30,39,42] and [40].

## 6. FOURIER EQUATIONS AND A MODEL PROBLEM

The well-known Fourier analysis/plane-wave expansion (PWE) method is briefly described here to fix the notation and make the paper self-contained. In 2D, the permittivity  $\epsilon(\mathbf{r})$  can, as a periodic function of coordinates, be expanded into a Fourier series with coefficients  $\tilde{\epsilon}_{\mathbf{m}}$

$$\epsilon(\mathbf{r}) = \sum_{\mathbf{m} \in \mathbb{Z}^2} \tilde{\epsilon}_{\mathbf{m}} \exp(i\mathbf{k}_{\mathbf{m}} \cdot \mathbf{r}). \quad (25)$$

For the Bloch–Floquet  $E$ -field, the negative of the Laplace operator turns, in the Fourier domain, into multiplication with  $|\mathbf{K}_B + \mathbf{k}_{\mathbf{m}}|^2$ . Furthermore, the product  $\epsilon \mathbf{E}$  of the wave equation turns into convolution, and thus the eigenvalue problem in Fourier space reads

$$|\mathbf{k}_{\mathbf{n}}|^2 e_{\mathbf{n}} = \omega^2 \mu_0 \sum_{\mathbf{m} \in \mathbb{Z}^2} \tilde{\epsilon}_{\mathbf{n}-\mathbf{m}} e_{\mathbf{m}}. \quad (26)$$

It is convenient to have a specific example in mind; however, the analysis and conclusions will be general. Consider the structure proposed by Gajic *et al.* [30] and Meisels *et al.* [31]. Their photonic crystal is a 2D square lattice of alumina rods in air (radius  $r_{\text{rod}} = 0.61$  mm and lattice constant  $a = 1.86$  mm). The band diagram for the  $s$ - and  $p$ -modes (Fig. 1) is computed using the plane-wave method with 441 waves and, apart from the scaling factors, is very close to the one in [30,31]. The TE2 dispersion curve is mildly convex around the  $\Gamma$  point ( $K_B = 0$ ,  $\omega a / 2\pi c \approx 0.427$ ), indicating a negative group velocity for small positive  $K_B$  and a possible backward wave. The distribution of Poynting components of the same wave is shown in Fig. 2. It is clear from Fig. 2 that the negative components outweigh the positive ones so that the power flows in the negative direction (see [40] for details).

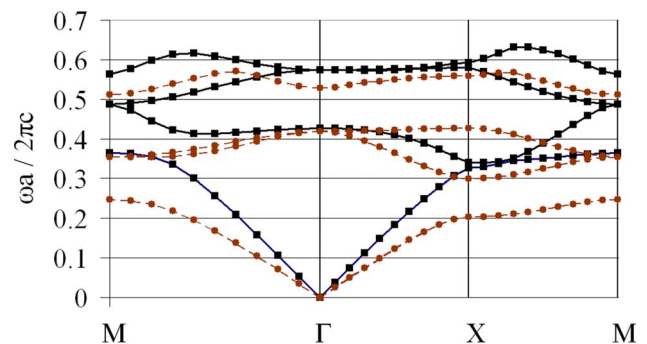


Fig. 1. (Color online) Photonic band diagram of the Gajic *et al.* crystal. TE modes ( $p$ -polarization, one-component  $H$ -field) (squares, bold curves). TM modes ( $s$ -polarization, one-component  $E$ -field) (circles, dashed curves).

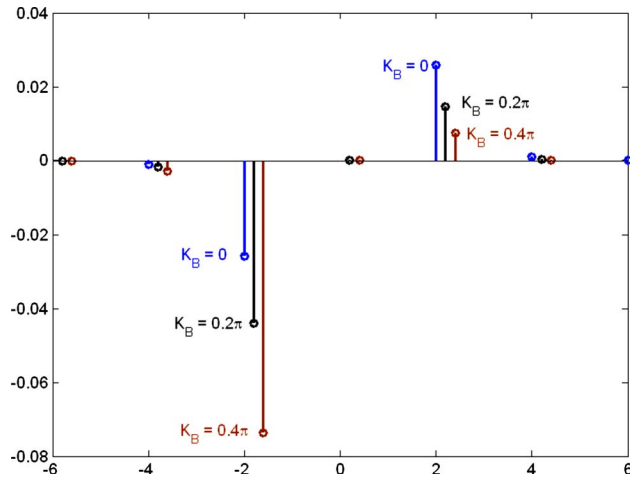


Fig. 2. (Color online) Plane-wave Poynting components  $P_n$  for the Gajic *et al.* crystal (arb. units). The TE2 mode near the  $\Gamma$  point on the  $\Gamma \rightarrow X$  line (From [40], p. 471, © 2008 Springer Science and Business Media, with kind permission of Springer Science and Business Media).

In the Gajic *et al.* [30] crystal, the amplitudes of the plane-wave harmonics for the TE2 mode are shown in Fig. 3. For  $K_B=0$  (i.e., at  $\Gamma$ ) the spectrum is symmetric and characteristic of a standing wave. As  $K_B$  becomes positive and increases, the spectrum gets skewed, with the backward components ( $K < 0$ ) increasing and the forward ones decreasing. The amplitudes of the spatial harmonics of this Bloch wave in the first-Brillouin-zone are quite small. In Section 7, we focus on cases where the first-Brillouin-zone component of the wave is pronounced and the structure consequently exhibits some qualitative characteristics of the Veselago medium.

## 7. LOWER BOUNDS FOR THE CELL SIZE

### A. Homogenization Limit

The following argument indicates that negative refraction disappears in the homogenization limit when the size of

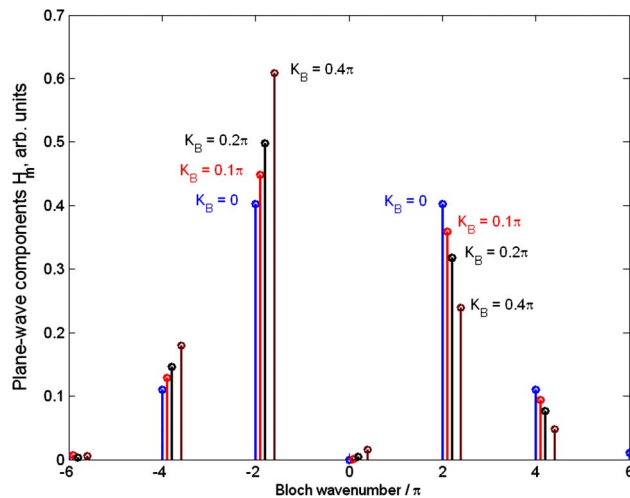


Fig. 3. (Color online) Amplitudes  $h_m$  of the plane-wave harmonics for the Gajic *et al.* crystal (arb. units). Second  $H$ -mode (TE2) near the  $\Gamma$  point on the  $\Gamma \rightarrow X$  line (From [40], p. 469, ©2008 Springer Science and Business Media, with kind permission of Springer Science and Business Media).

the lattice cells tends to zero, provided that other physical parameters, including frequency, are fixed.

It is natural to normalize the coordinates as  $\tilde{x}=x/a$ ,  $\tilde{y}=y/a$ ,  $\tilde{z}=z/a$  so that in the tilde-coordinates the 2D/3D problem is set up in the unit square/cube and the governing equations become, in 2D and 3D, respectively,

$$\tilde{\nabla}^2 E + \tilde{\omega}^2 \epsilon E = 0, \quad (27)$$

$$\tilde{\nabla} \times \tilde{\nabla} \times \mathbf{E} = \tilde{\omega}^2 \epsilon(\mathbf{r}) \mathbf{E}, \quad (28)$$

$$\tilde{\nabla} \times \epsilon^{-1}(\mathbf{r}) \tilde{\nabla} \times \mathbf{H} = \tilde{\omega}^2 \mathbf{H}, \quad (29)$$

where  $c$ ,  $k_0$ , and  $\lambda_0$  are the speed of light, the wavenumber, and the wavelength in a vacuum, respectively;  $\epsilon$  is now the relative permittivity,  $\tilde{\omega} = \omega a / c = k_0 a$ .

When converted to Fourier space, Eq. (27) becomes a normalized version of Eq. (26),

$$|\tilde{\mathbf{K}}_B + 2\pi\mathbf{m}|^2 e_{\mathbf{n}} = \tilde{\omega}^2 \sum_{\mathbf{m} \in \mathbb{Z}^2} \tilde{\epsilon}_{\mathbf{n}-\mathbf{m}} e_{\mathbf{m}}. \quad (30)$$

The left hand side is the Fourier representation of  $-\tilde{\nabla}^2$  and the right hand side is convolution corresponding to the product  $\epsilon E$ .

The homogenization limit (small cell size, long-wavelength) is  $a \rightarrow 0$ ,  $\tilde{K}_B = K_B a \rightarrow 0$ . (Sjöberg *et al.* [43] provide additional mathematical details on the Floquet-based homogenization theory for Maxwell's equations.) As these limits are taken, the problem and the dispersion curves in the normalized coordinates remain unchanged, and the reference point  $(\tilde{\omega}, \tilde{\mathbf{K}})$  approaches the origin along a fixed dispersion curve, the acoustic branch. In the example of Fig. 1, the acoustic branch is clearly identifiable as two approximately straight lines originating from the  $\Gamma$  point.

Around the  $\Gamma$  point, phase velocity in any given direction  $\hat{l}$ ,  $\omega/K_l = \tilde{\omega}/\tilde{K}_l$  is well defined and equal to group velocity  $\partial\omega/\partial K_l$  simply by definition of the derivative. No backward waves can be supported in this regime. This argument suggests that the relative cell size  $a/\lambda_0$  of a periodic structure with backward waves must lie above a certain threshold. To the best of my knowledge, this question is currently open and has not even been explicitly posed in literature except for [40].

The existence of a lower bound on the cell size for photonic crystals is not surprising as they are in any event expected to have features not much smaller than the wavelength. For metamaterials, the situation is more interesting, and the cell size limit has a physical explanation. Indeed, the principal component of artificial metamaterials with negative refraction is some resonating element [4,9,17,18], and the resonance frequency is, roughly, inverse proportional to size (Linden *et al.* [38] and Tretyakov [44]). As the size of the lattice cell diminishes, the operating frequency increases so that it is not the absolute frequency  $\omega$  but the normalized quantity  $\tilde{\omega}$  that remains (approximately) constant. If the absolute frequency were to be fixed as the cell size decreases, the

resonance would peter out and the backward waves would disappear in accordance with the general argument above.

### B. Definition of the Weakly Inhomogeneous Backward-Wave (Veselago) Regime

The rationale for the following set of conditions is to make the Bloch wave in an artificial structure resemble, to the extent possible, a plane wave in an ideal Veselago medium.

1. The Bloch wave in the metamaterial is, in some sense, close to a long-wavelength plane wave.
2. In particular, the plane-wave component in the first-Brillouin-zone is dominant. It is this component that defines the phase velocity of the Bloch wave.
3. Other plane-wave components collectively produce energy flow at an obtuse angle with phase velocity.
4. At the air-material interface, it is the long-wavelength, first-Brillouin-zone component that serves as the excitation channel for the Bloch wave.

By this definition, the “Veselago regime” corresponds to small values of  $\tilde{K}_B$  ( $\tilde{K}_B = K_B a \ll \pi$ ). Larger values of  $\tilde{K}_B$  indicate a photonic crystal or grating regime, where the lattice size is comparable with the Bloch wavelength. This is a case of strong inhomogeneity in the sense that the wave can “see” the microstructure of the medium. It is known (e.g., Notomi [23], Cubukcu *et al.* [25]) that negative refraction is possible in such cases.

In the remainder, we investigate the constraints on the periodic structure in the weakly inhomogeneous backward-wave regime as defined above. This implies long Bloch wavelengths,  $\tilde{K}_B = K_B a \ll 1$ . To simplify the mathematical analysis, we focus on the limiting case  $K_B = 0$ , but the conclusions will apply, by physical continuity, to small  $\tilde{K}_B$ . Moreover, only media with low losses at the operating frequency are of practical interest; large losses would quench all propagating modes. (Stockman [45] showed that for linear homogeneous negative-index media large losses *close* to the operating frequency are unavoidable as a matter of principle; this follows from causality relations.)

In the absence of losses,  $\epsilon$  is real and may be positive or negative. The estimates below depend on the average value of  $\epsilon$  over the lattice cell or equivalently on the Fourier coefficient  $\tilde{\epsilon}_0$ . It will be assumed that this average value is *not* close to zero; this assumption covers the majority of practical situations. (The effective  $\epsilon$  of the double-negative medium, assuming that this value can be adequately defined [46], must be negative but does not have to be equal to  $\tilde{\epsilon}_0$ .) The case  $\tilde{\epsilon}_0 = 0$  is mathematically quite involved and left for future studies.

### C. Power Flow for Long Bloch Wavelengths

To establish a lower bound for the cell size of a negative-index structure, we first turn to the 1D case for mathematical simplicity. The  $E$ -field in the normalized coordinate  $\tilde{x}$  is expressed via Fourier harmonics as

$$E(\tilde{x}) = \sum_{m \in \mathbb{Z}} e_m \exp(i2\pi m \tilde{x}). \quad (31)$$

It is instructive to examine the direction of power flow. The average Poynting vector is, according to Eq. (24) and with a convenient normalization,

$$\begin{aligned} \tilde{P} &\equiv 2\omega\mu_0\alpha(P) = \tilde{K}_B |e_0(\tilde{K}_B)|^2 \\ &+ \sum_{m=1}^{\infty} (\tilde{K}_B + 2\pi m) |e_m(\tilde{K}_B)|^2 + (\tilde{K}_B - 2\pi m) |e_{-m}(\tilde{K}_B)|^2. \end{aligned} \quad (32)$$

Here it is essential to explicitly indicate that the Fourier amplitudes  $e_m$  depend on the Bloch parameter  $\tilde{K}_B$ . Since the waves corresponding to  $\pm\tilde{K}_B$  are, in the lossless case (real  $\epsilon$ ), complex conjugates of one another, we have  $e_{-m}(\tilde{K}_B) = e_m^*(-\tilde{K}_B)$ , and the expression for the Poynting vector becomes

$$\begin{aligned} \tilde{P} &= \tilde{K}_B |e_0(\tilde{K}_B)|^2 + \sum_{m=1}^{\infty} (\tilde{K}_B + 2\pi m) |e_m(\tilde{K}_B)|^2 \\ &+ (\tilde{K}_B - 2\pi m) |e_m(-\tilde{K}_B)|^2 \\ &= \tilde{K}_B |e_0(\tilde{K}_B)|^2 + \tilde{K}_B \sum_{m=1}^{\infty} (|e_m(\tilde{K}_B)|^2 + |e_m(-\tilde{K}_B)|^2) \\ &+ 2\pi \sum_{m=1}^{\infty} m (|e_m(\tilde{K}_B)|^2 - |e_m(-\tilde{K}_B)|^2). \end{aligned} \quad (33)$$

The first two terms in Eq. (33) are directly proportional to  $\tilde{K}_B$ . To make this small parameter explicit in the third sum as well let us write

$$\begin{aligned} \tilde{P} &= \tilde{K}_B \left[ |e_0|^2 + \sum_{m=1}^{\infty} (|e_m(\tilde{K}_B)|^2 + |e_m(-\tilde{K}_B)|^2) \right. \\ &\left. + 2\pi \sum_{m=1}^{\infty} m \frac{\partial e_m^2}{\partial \tilde{K}_B} \right]. \end{aligned} \quad (34)$$

A critical observation is that for small  $\tilde{\omega}$ , the expression in the large brackets tends to be dominated by  $|e_0|^2$  and to be positive, making the backward-wave phenomenon difficult to achieve. Indeed, the eigenproblem of Eq. (30) for small  $\tilde{\omega}$  constrains the values of all Fourier harmonics with the exception of  $e_0$ ,

$$\begin{aligned} |e_n| &= \tilde{\omega}^2 (\tilde{K}_B + 2\pi n)^{-2} \left| \sum_{m \in \mathbb{Z}} \epsilon_{n-m} e_m \right| \\ &\leq \tilde{\omega}^2 (\tilde{K}_B + 2\pi n)^{-2} \|\epsilon\|_{l_2} \|e\|_{l_2}, \quad n \neq 0, \end{aligned} \quad (35)$$

where the  $l_2$ -norm, standard for infinite sequences, is analogous to the Euclidean norm for finite-dimensional vectors.

#### D. Cell Size Bounds for the E-Mode

For  $\tilde{\omega} \neq 0$  and  $\eta = \tilde{\omega}^{-2}$ ,

$$\epsilon \mathbf{E} = -\eta \tilde{\nabla}^2 \mathbf{E}. \quad (36)$$

Further analysis relies on the inversion of  $\tilde{\nabla}^2$ . To unambiguously do this, let us split  $\mathbf{E}$  up into the zero-mean term  $\mathbf{E}_\perp$  and the remaining constant  $\mathbf{E}_0$ ,  $\mathbf{E} = \mathbf{E}_0 + \mathbf{E}_\perp$ . The symbol “ $\perp$ ” indicates orthogonality (in the functional analysis sense) to the null space of the Laplacian (i.e., to constants). To eliminate the constant component  $\mathbf{E}_0$ , we integrate Eq. (36) over the lattice cell. Integrating by parts and noting that the boundary term vanishes due to the periodic boundary conditions ( $K_B = 0$ ) we get

$$\mathbf{E}_0 = -\tilde{\epsilon}_0^{-1} \int_{\Omega} \epsilon \mathbf{E}_\perp d\Omega, \quad \tilde{\epsilon}_0 \neq 0.$$

(The exceptional case  $\tilde{\epsilon}_0 = 0$  is mathematically quite intricate and constitutes a special topic for future research.) With  $\mathbf{E}_0$  eliminated, the eigenvalue problem for  $\mathbf{E}_\perp$  becomes

$$\epsilon \left[ \mathbf{E}_\perp - \tilde{\epsilon}_0^{-1} \int_{\Omega} \epsilon \mathbf{E}_\perp d\Omega \right] = -\eta \tilde{\nabla}^2 \mathbf{E}_\perp.$$

Since  $\mathbf{E}_\perp$  by definition is zero-mean,

$$\tilde{\nabla}_\perp^{-2} \{ \epsilon [\mathbf{E}_\perp - \tilde{\epsilon}_0^{-1} \int_{\Omega} \epsilon \mathbf{E}_\perp d\Omega] \} = -\eta \mathbf{E}_\perp, \quad (37)$$

where  $\tilde{\nabla}_\perp^{-2}$  is the zero-mean inverse of the Laplacian. Fourier analysis easily shows that this inverse is bounded (the Poincaré inequality),  $\|\tilde{\nabla}_\perp^{-2}\| \leq (4\pi^2)^{-1}$ . Then, taking the norm of both sides of Eq. (37) we get

$$|\eta| \leq (4\pi^2)^{-1} |\epsilon|_{\max} \left( 1 + \frac{|\epsilon|_{\max}}{|\tilde{\epsilon}_0|} \right). \quad (38)$$

This result, which can be viewed as a generalization of the Poincaré inequality to cases with variable  $\epsilon$ , leads to a simple lower bound for the lattice cell size with the mean and maximum values of  $\epsilon$  as parameters,

$$\left( \frac{a}{\lambda_0} \right)^2 = \frac{\tilde{\omega}^2}{4\pi^2} \geq |\epsilon|_{\max}^{-1} (1 + |\tilde{\epsilon}_0|^{-1} |\epsilon|_{\max})^{-1}. \quad (39)$$

This is the main result for the 1D case.

#### E. Cell Size Bounds for the General Case

Turning now to the vector field formulation of Eq. (15), we simultaneously deal with 2D and 3D cases and rewrite the field equation as

$$\epsilon \mathbf{E} = \eta \tilde{\nabla} \times \tilde{\nabla} \times \mathbf{E}. \quad (40)$$

The  $\tilde{\nabla} \times \tilde{\nabla} \times$  operator can be unambiguously inverted if the result, denoted with  $(\tilde{\nabla} \times)_\perp^{-2}$ , is sought in the functional space  $\mathbf{H}_\perp^1(\Omega)$  of divergence-free zero-mean fields. For any such field  $\mathbf{u}$ ,  $\tilde{\nabla} \times \tilde{\nabla} \times \mathbf{u} = -\tilde{\nabla}^2 \mathbf{u}$  and hence

$$\begin{aligned} \|\tilde{\nabla}^2 \mathbf{u}\|_2^2 &= (\tilde{\nabla} \times \tilde{\nabla} \times \mathbf{u}, \tilde{\nabla} \times \tilde{\nabla} \times \mathbf{u}) = (\tilde{\nabla}^2 \mathbf{u}, \tilde{\nabla}^2 \mathbf{u}) \\ &\geq (4\pi^2)^2 (\mathbf{u}, \mathbf{u}) = (4\pi^2)^2 \|\mathbf{u}\|_2^2. \end{aligned}$$

This implies that the inverse curl-curl, considered as an operator with its range in  $\mathbf{H}_\perp^1$ , is bounded

$$\|(\tilde{\nabla} \times)_\perp^{-2}\| \leq (4\pi^2)^{-1}. \quad (41)$$

The relevant splitting of  $\mathbf{E}$  is into the zero-mean divergence-free term  $\mathbf{E}_\perp \in \mathbf{H}_\perp^1$  and the curl-free remainder  $\mathbf{E}_0 = -\nabla \phi_0$  (the Helmholtz decomposition),  $\mathbf{E} = \mathbf{E}_\perp - \tilde{\nabla} \phi_0$ . (Curl-free fields are representable as gradients if the domain is simply connected, which is certainly true for any Bravais lattice cell.) Field  $\mathbf{E}_\perp$  is in fact, up to the factor  $i\tilde{\omega}$ , the magnetic vector potential with the Coulomb (zero-divergence) gauge.

Taking divergence (in the distributional sense) of the governing Eq. (40) and integrating over the cell, one eliminates the electrostatic term  $\tilde{\nabla} \phi_0$  and arrives at an eigenvalue problem for  $\mathbf{E}_\perp$ ,

$$\epsilon (\mathbf{E}_\perp - \nabla \mathcal{L}_\epsilon^{-1} \tilde{\nabla} \cdot (\epsilon \mathbf{E}_\perp)) = \eta \tilde{\nabla} \times \tilde{\nabla} \times \mathbf{E}_\perp,$$

assuming that the electrostatic operator  $\mathcal{L}_\epsilon = \tilde{\nabla} \cdot \epsilon \tilde{\nabla}$  is nonsingular. Equivalently, since  $\mathbf{E}_\perp$  is by definition divergence-free and zero-mean,

$$(\tilde{\nabla} \times)_\perp^{-2} \{ \epsilon [\mathbf{E}_\perp - \nabla \mathcal{L}_\epsilon^{-1} \tilde{\nabla} \cdot (\epsilon \mathbf{E}_\perp)] \} = \eta \mathbf{E}_\perp. \quad (42)$$

An upper bound for  $\eta$  can be obtained by taking the  $\mathbf{L}_2$ -norms of both sides with Eq. (41) in mind,

$$|\eta| \leq (4\pi^2)^{-1} |\epsilon|_{\max} (1 + |\lambda|_{\max}(\mathcal{L}_\epsilon^{-1}) |\epsilon|_{\max}). \quad (43)$$

This estimate is analogous to the scalar one of Eq. (38), except that the maximum eigenvalue  $|\lambda|_{\max}(\mathcal{L}_\epsilon^{-1})$  (not to be confused with the wavelength) replaces the inverse mean value  $|\tilde{\epsilon}_0|^{-1}$  of the permittivity. This eigenvalue is bounded unless the operating frequency is close to the quasi-static plasmon resonance value. In the most general situation, no simple estimate of  $|\lambda|_{\max}(\mathcal{L}_\epsilon^{-1})$  is available, but it can be numerically computed using a number of algorithms (see, e.g., [40]) for any given distribution of  $\epsilon$  in the lattice cell.

At the same time, there are practically important situations where the bound for  $\eta$  can be made more explicit. One such case is that of nonplasmonic materials when  $\epsilon \geq \epsilon_{\min} > 0$  throughout the lattice cell. Then

$$|\lambda|_{\max}(\mathcal{L}_\epsilon^{-1}) \leq \epsilon_{\min}^{-1} |\lambda|_{\max}(\nabla_\perp^{-2}) \leq (4\pi^2 \epsilon_{\min})^{-1}$$

and from the estimate of Eq. (43) for  $|\eta|$  the following bound on the normalized cell size emerges:

$$\left( \frac{a}{\lambda_0} \right)^2 = \left( \frac{\tilde{\omega}}{2\pi} \right)^2 = \frac{1}{4\pi^2 |\eta|} \geq \frac{1}{|\epsilon|_{\max} (1 + |\epsilon|_{\max} / (4\pi^2 \epsilon_{\min}))}. \quad (44)$$

Another case where the theoretical bound of Eq. (43) can be made more explicit is that of a lossless host medium,  $\epsilon = \epsilon_h$ , with embedded “inclusions”  $\epsilon = \epsilon_i = \epsilon'_i + i\epsilon''_i$  (spheres, SRRs, fishnets, horseshoes, rods, etc.). The eigenvalue  $|\lambda|_{\max}(\mathcal{L}_\epsilon^{-1}) = |\lambda|_{\min}^{-1}(\mathcal{L}_\epsilon)$  can be estimated from the electrostatic energy functional

$$(\epsilon \nabla \phi, \nabla \phi) = \epsilon_h W_h + (\epsilon'_i + i \epsilon''_i) W_i,$$

where  $W_{h,i} = \int_{\Omega_{h,i}} |\nabla \phi|^2 d\Omega$ . Then noting that  $|(\epsilon \nabla \phi, \nabla \phi)|^2$  is a quadratic form with respect to  $W_{h,i}$ , one can show that

$$|\lambda|_{\max}(\mathcal{L}_\epsilon^{-1}) \leq \frac{\sqrt{(\epsilon_h - \epsilon'_i)^2 + \epsilon''_i{}^2}}{4\pi^2 \epsilon_h \epsilon''_i}.$$

This estimate can be used in conjunction with the general bound of Eq. (43).

**F. Numerical Illustration**

The lower bounds of Eqs. (39) and (44) are plotted as a function of  $|\epsilon|_{\max}$  in Fig. 4 for  $\epsilon_{\min} = 1$  and two different values of  $\tilde{\epsilon}_0$  (0.5 and 0.1). For illustration, several representative data points (both theoretical and experimental) from literature are also shown in Fig. 4. As an approximation, no distinction is made between different Bravais lattices, even though for cells other than squares and cubes the numerical factors such as  $4\pi^2$  in Eq. (44) would, strictly speaking, need to be adjusted.

In the microwave regime, when metals are very good conductors and consequently  $|\epsilon|_{\max}$  is high, the theoretical bound for the cell size is nonrestrictive and the respective data points (due to Smith, Shelby, Houck, and others) easily turn up above the relevant theoretical curve; these points lie off the chart in Fig. 4.

The Cubukcu *et al.* [25] data point lies below the theoretical line of Eq. (44); however, there is no contradiction because in this instance negative refraction occurs in the vicinity of the *M* point, where the Bloch wavelength and the lattice cell size are comparable. This constitutes, by our definition, a strongly inhomogeneous case while the theoretical bounds apply to the weakly inhomogeneous (Veselago) regime as defined in Subsection 7.B.

The Moussa and Gajic data points for nonmetallic crystals lie only slightly above the theoretical bound, indicating that this bound can be approached in some cases. Still, it must be stressed that the theoretical limits on the cell size are necessary, but in general not sufficient, conditions for negative refraction. A sufficiently large lattice cell size makes it possible for higher-order Fourier harmonics of the Bloch wave to outweigh the first-Brillouin-zone harmonic but does not guarantee that they will do so and that they will have the desirable sign.

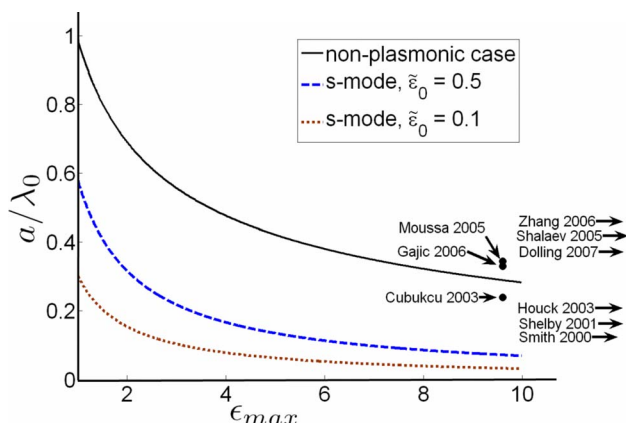


Fig. 4. (Color online) Bounds on the normalized cell size and a few representative data points from the literature.

**G. Implications for Imaging**

The Pendry–Veselago “perfect lens” (a slab of a hypothetical lossless and homogeneous medium with index  $n = -1$  [10]) is in principle capable of producing ideal images. In reality, there are several sources of imperfection, such as losses (affecting the resolution with a logarithmic factor of  $\sim \log(\epsilon''/2)$  [47,48]), surface roughness, nonlocality of the dielectric response [49,50], and the granularity of the structure.

The latter constraint is intimately related to the subject of this paper. According to Smith *et al.* [48], in the long-wavelength regime with  $a\Delta/\lambda_0 \ll 1$ , where  $\Delta$  characterizes the deviation of the index from its perfect lens value of  $-1$ , the resolution-limiting factor is  $\log(\lambda_0/(a\Delta^2))$  (see also Luo *et al.* [51] for the photonic crystal case). Therefore the bounds of Section 7 on the lattice size  $a$  immediately translate into constraints on the maximum optical resolution achievable with a negative-index lens.

**H. NonPeriodic Media**

As noted by the anonymous reviewer, an interesting open question is whether or not similar lower bounds exist for the cell size of nonperiodic negative-index media. The answer is very likely to be positive. One case in point is due to Alù *et al.* [52], nanorings of dielectric particles in a host dielectric may produce a medium with nontrivial effective electric and magnetic characteristics  $\epsilon_{\text{eff}}$  and  $\mu_{\text{eff}}$ , including (under suitable resonance conditions) a negative effective index. However, asymptotic analysis yields  $\mu_{\text{eff}} \sim 1 + \mathcal{O}((R/\lambda_b)^2)$ , where  $R$  is the radius of the nanoring and  $\lambda_b$  is the wavelength in the background medium. Hence nontrivial effects can only arise if the radius of the ring is a sufficiently large fraction of the wavelength.

**8. SUMMARY**

The Fourier–Bloch decomposition of the field into plane-wave components clarifies the nature of backward waves. Phase velocity is primarily governed by the first-Brillouin-zone component of the Bloch wave, assuming that this component has an appreciable magnitude. In contrast, energy flow is a collective effect of all plane-wave harmonics. Backward waves occur when higher-order harmonics, taken together, outweigh the first one and have the opposite sign.

Intrinsic and extrinsic characteristics should be distinguished. The forward or backward character of a wave is its intrinsic characteristic in the bulk of the material. At interface boundaries, the Bloch wave can in principle be excited via any of its plane-wave components. The type of refraction depends on both factors, the intrinsic character of the wave and the excitation channel.

One might think that an artificial periodic structure could approach an ideal backward-wave Veselago medium if the lattice cell size becomes vanishingly small. However, as the cell size tends to zero, the operating point on the normalized band diagram of the structure falls on the acoustic branch, thereby eliminating the difference between phase and group velocities.

More specifically, if a periodic structure were to resemble an ideal Veselago medium with backward waves, it would need to be weakly inhomogeneous as defined

more precisely in Subsection 7.B. Furthermore, the lattice cell size, as a fraction of the vacuum wavelength, must be above certain thresholds. These thresholds, explicitly established in this paper, depend on the maximum, minimum, and mean values of the complex dielectric permittivity as key parameters. In the presence of good conductors (e.g., at microwave frequencies) such theoretical constraints are not too restrictive. However, at optical frequencies and/or for nonmetallic structures the bounds on the cell size must be honored and may help to design artificial periodic structures with desired optical properties.

Finally, the plasmonic case is an intriguing exception, as evidenced by the presence of the inverse electrostatic operator in the cell size bounds; this is consistent with the previous analytical and numerical work of Shvets *et al.* [53,54].

## ACKNOWLEDGMENTS

I thank Frantisek Čajko for his perceptive comments, Dmitry Golovaty for reading the manuscript and discussing some mathematical issues, Alain Bossavit for interesting questions, and the anonymous reviewer for helpful remarks. I am grateful to N.-A. Nicorovici, G. W. Milton, and G. Shvets for bringing several important references to my attention.

## REFERENCES

- J. B. Pendry and D. R. Smith, "Reversing light with negative refraction," *Phys. Today* **57**, 37–43 (2004).
- P. W. Milonni, *Fast Light, Slow Light and Left-Handed Light* (Taylor & Francis, 2004).
- G. V. Eleftheriades and K. G. Balmain, *Negative Refraction Metamaterials: Fundamental Principles and Applications* (Wiley-IEEE Press, 2005).
- S. A. Ramakrishna, "Physics of negative refractive index materials," *Rep. Prog. Phys.* **68**, 449–521 (2005).
- L. I. Mandelshtam, "Group velocity in crystalline arrays," *Zh. Eksp. Teor. Fiz.* **15**, 475–478 (1945).
- L. I. Mandelshtam, *Polnoe Sobranie Trudov*, Vol. 2.5 (Akademiia Nauk SSSR, 1947, 1950).
- V. G. Veselago, "Electrodynamics of substances with simultaneously negative values of  $\epsilon$  and  $\mu$ ," *Sov. Phys. Usp.* **10**, 509–514 (1968).
- J. B. Pendry, A. J. Holden, D. J. Robbins, and W. J. Stewart, "Magnetism from conductors and enhanced nonlinear phenomena," *IEEE Trans. Microwave Theory Tech.* **47**, 2075–2084 (1999).
- D. R. Smith, W. J. Padilla, D. C. Vier, S. C. Nemat-Nasser, and S. Schultz, "Composite medium with simultaneously negative permeability and permittivity," *Phys. Rev. Lett.* **84**, 4184–4187 (2000).
- J. B. Pendry, "Negative refraction makes a perfect lens," *Phys. Rev. Lett.* **85**, 3966–3969 (2000).
- N. A. Nicorovici, R. C. McPhedran, and G. W. Milton, "Optical and dielectric properties of partially resonant composites," *Phys. Rev. B* **49**, 8479–8482 (1994).
- G. W. Milton and N.-A. P. Nicorovici, "On the cloaking effects associated with anomalous localized resonance," *Proc. R. Soc. London, Ser. A* **462**, 3027–3059 (2006).
- G. W. Milton, N.-A. P. Nicorovici, R. C. McPhedran, and V. A. Podolskiy, "A proof of superlensing in the quasistatic regime and limitations of superlenses in this regime due to anomalous localized resonance," *Proc. R. Soc. London, Ser. A* **461**, 3999–4034 (2005).
- R. A. Shelby, D. R. Smith, and S. Schultz, "Experimental verification of a negative index of refraction," *Science* **292**, 77–79 (2001).
- C. G. Parazzoli, R. B. Greegor, K. Li, B. E. C. Koltenbah, and M. Tanielian, "Experimental verification and simulation of negative index of refraction using Snell's law," *Phys. Rev. Lett.* **90**, 107401 (2003).
- A. A. Houck, J. B. Brock, and I. L. Chuang, "Experimental observations of a left-handed material that obeys Snell's law," *Phys. Rev. Lett.* **90**, 137401 (2003).
- D. R. Smith and D. C. Vier, "Design of metamaterials with negative refractive index," *Proc. SPIE* **5359**, 52–63 (2004).
- V. M. Shalaev, "Optical negative-index metamaterials," *Nat. Photonics* **1**, 41–48 (2007).
- S. Zhang, W. Fan, K. J. Malloy, S. R. J. Brueck, N. C. Panoiu, and R. M. Osgood, "Demonstration of metal-dielectric negative-index metamaterials with improved performance at optical frequencies," *J. Opt. Soc. Am. B* **23**, 434–438 (2006).
- G. Dolling, C. Enkrich, M. Wegener, C. M. Soukoulis, and S. Linden, "Low-loss negative-index metamaterial at telecommunication wavelengths," *Opt. Lett.* **31**, 1800–1802 (2006).
- G. Dolling, M. Wegener, C. M. Soukoulis, and S. Linden, "Negative-index metamaterial at 780 nm wavelength," *Opt. Lett.* **32**, 53–55 (2007).
- R. Zengerle, "Light propagation in singly and doubly periodic planar waveguides," *J. Mod. Opt.* **34**, 1589–1617 (1987).
- M. Notomi, "Theory of light propagation in strongly modulated photonic crystals: refraction like behavior in the vicinity of the photonic band gap," *Phys. Rev. B* **62**, 10696–10705 (2000).
- C. Luo, S. G. Johnson, J. D. Joannopoulos, and J. B. Pendry, "All-angle negative refraction without negative effective index," *Phys. Rev. B* **65**, 201104 (2002).
- E. Cubukcu, K. Aydin, E. Ozbay, S. Foteinopolou, and C. M. Soukoulis, "Subwavelength resolution in a two-dimensional photonic-crystal-based superlens," *Phys. Rev. Lett.* **91**, 207401 (2003).
- R. Moussa, S. Foteinopolou, L. Zhang, G. Tuttle, K. Guven, E. Ozbay, and C. M. Soukoulis, "Negative refraction and superlens behavior in a two-dimensional photonic crystal," *Phys. Rev. B* **71**, 085106 (2005).
- V. Yannopapas and A. Moroz, "Negative refractive index metamaterials from inherently non-magnetic materials for deep infrared to terahertz frequency ranges," *J. Phys. Condens. Matter* **17**, 3717–3734 (2005).
- M. S. Wheeler, J. S. Aitchison, and M. Mojahedi, "Coated nonmagnetic spheres with a negative index of refraction at infrared frequencies," *Phys. Rev. B* **73**, 045105 (2006).
- P. V. Parimi, W. T. Lu, P. Vodo, J. Sokoloff, J. S. Derov, and S. Sridhar, "Negative refraction and left-handed electromagnetism in microwave photonic crystals," *Phys. Rev. Lett.* **92**, 127401 (2004).
- R. Gajic, R. Meisels, F. Kuchar, and K. Hingerl, "Refraction and rightness in photonic crystals," *Opt. Express* **13**, 8596–8605 (2005).
- R. Meisels, R. Gajic, F. Kuchar, and K. Hingerl, "Negative refraction and flat-lens focusing in a 2d square-lattice photonic crystal at microwave and millimeter wave frequencies," *Opt. Express* **14**, 6766–6777 (2006).
- A. L. Pokrovsky and A. L. Efros, "Sign of refractive index and group velocity in lefthanded media," *Solid State Commun.* **124**, 283–287 (2002).
- R. W. Ziolkowski and E. Heyman, "Wave propagation in media having negative permittivity and permeability," *Phys. Rev. E* **64**, 056625 (2001).
- M. W. McCall, A. Lakhtakia, and W. S. Weiglhofer, "The negative index of refraction demystified," *Eur. J. Phys.* **23**, 353–359 (2002).
- R. A. Depine and A. Lakhtakia, "A new condition to identify isotropic dielectric-magnetic materials displaying negative phase velocity," *Microwave Opt. Technol. Lett.* **41**, 315–316 (2004).

36. L. D. Landau and E. M. Lifshitz, *Electrodynamics of Continuous Media* (Pergamon, 1984).
37. W. Cai, U. K. Chettiar, H.-K. Yuan, V. C. de Silva, A. V. Kildishev, V. P. Drachev, and V. M. Shalaev, "Metamagnetics with rainbow colors," *Opt. Express* **15**, 3333–3341 (2007).
38. S. Linden, C. Enkrich, G. Dolling, M. W. Klein, J. Zhou, T. Koschny, C. M. Soukoulis, S. Burger, F. Schmidt, and M. Wegener, "Photonic metamaterials: magnetism at optical frequencies," *IEEE J. Sel. Top. Quantum Electron.* **12**, 1097–1105 (2006).
39. B. Lombardet, L. A. Dunbar, R. Ferrini, and R. Houdré, "Fourier analysis of Bloch wave propagation in photonic crystals," *J. Opt. Soc. Am. B* **22**, 1179–1190 (2005).
40. I. Tsukerman, *Computational Methods for Nanoscale Applications: Particles, Plasmons and Waves* (Springer, 2008).
41. P. Yeh, "Electromagnetic propagation in birefringent layered media," *J. Opt. Soc. Am.* **69**, 742–756 (1979).
42. P. A. Belov, C. R. Simovski, and S. A. Tretyakov, "Backward waves and negative refraction in photonic (electromagnetic) crystals," *J. Commun. Technol. Electron.* **49**, 1199–1207 (2004).
43. D. Sjöberg, C. Engstrom, G. Kristensson, D. J. N. Wall, and N. Wellander, "A Floquet–Bloch decomposition of Maxwell's equations applied to homogenization," *Multiscale Model. Simul.* **4**, 149–171 (2005).
44. S. Tretyakov, "On geometrical scaling of split-ring and double-bar resonators at optical frequencies," *Metamaterials* **1**, 40–43 (2007).
45. M. I. Stockman, "Criterion for negative refraction with low optical losses from a fundamental principle of causality," *Phys. Rev. Lett.* **98**, 177404 (2007).
46. D. R. Smith and J. B. Pendry, "Homogenization of metamaterials by field averaging," *J. Opt. Soc. Am. B* **23**, 391–403 (2006).
47. R. Merlin, "Analytical solution of the almost-perfect-lens problem," *Appl. Phys. Lett.* **84**, 1290–1292 (2004).
48. D. R. Smith, D. Schurig, M. Rosenbluth, S. Schultz, S. A. Ramakrishna, and J. B. Pendry, "Limitations on subdiffraction imaging with a negative refractive index slab," *Appl. Phys. Lett.* **82**, 1506–1508 (2003).
49. F. D. M. Haldane, "Electromagnetic surface modes at interfaces with negative refractive index make a not-quite-perfect lens," arXiv:cond-mat/0206420v3 (2002).
50. I. A. Larkin and M. I. Stockman, "Imperfect perfect lens," *Nano Lett.* **5**, 339–343 (2005).
51. C. Luo, S. G. Johnson, J. D. Joannopoulos, and J. B. Pendry, "Subwavelength imaging in photonic crystals," *Phys. Rev. B* **68**, 045115 (2003).
52. A. Alù, A. Salandrino, and N. Engheta, "Negative effective permeability and left-handed materials at optical frequencies," *Opt. Express* **14**, 1557–1567 (2006).
53. G. Shvets and Y. A. Urzhumov, "Engineering the electromagnetic properties of periodic nanostructures using electrostatic resonances," *Phys. Rev. Lett.* **93**, 243902 (2004).
54. M. Davanço, Y. Urzhumov, and G. Shvets, "The complex Bloch bands of a 2D plasmonic crystal displaying isotropic negative refraction," *Opt. Express* **15**, 9681–9691 (2007).